How large is the [Fe(III)(protoporphyrin IX)]+ ion (hemin+) in the gas phase?

ARTICLE *in* THE JOURNAL OF PHYSICAL CHEMISTRY B · DECEMBER 2006

Impact Factor: 3.3 · DOI: 10.1021/jp064873c · Source: PubMed

4 AUTHORS, INCLUDING:

Chi-Kit Siu
City University of Hong Kong
59 PUBLICATIONS **732** CITATIONS

SEE PROFILE

How Large Is the [Fe^{III}(Protoporphyrin IX)]$^+$ Ion (Hemin$^+$) in the Gas Phase?

Chi-Kit Siu, Yuzhu Guo, Alan C. Hopkinson, and K. W. Michael Siu*

Department of Chemistry and Centre for Research in Mass Spectrometry, York University, 4700 Keele Street, Toronto, Ontario, Canada M3J 1P3

Received: July 30, 2006; In Final Form: September 7, 2006

Comparison of the collision cross-section of the [Fe^{III}−protoporphyrin IX]$^+$ ion, hemin$^+$, measured by means of ion-mobility experiments and the cross-sections calculated from theoretical structures based on density functional theory reveals that hemin$^+$, in the gas phase, contains intramolecular hydrogen bonding between its two propionic acid side-chains.

Introduction

Iron−protoporphyrin IX is the prosthetic group in hemeproteins that performs important biological functions, such as oxygen transport by hemoglobin in the red blood cells and oxygen storage by myoglobin in muscle tissues. Figure 1a shows the structure of iron−protoporphyrin IX. The iron ion, as in the 2+ (heme) or 3+ (hemin$^+$) oxidation state, is 4-coordinate with a square planar geometry surrounded by four pyrrole nitrogen atoms. The axial positions are unhindered and can bind two additional ligands. The coordination chemistry depends on the structural details of the protein and its environment. Isolating the hemin$^+$ complex in the gas-phase eliminates solvent effects and permits probing into the complex's intrinsic properties, for example, its inherent stability and fragmentation reactions,[1,2] its coordination chemistry,[2,3] and its suitability as a model for biological compounds.[4]

Within a protein framework, hemin$^+$ can bind specific protein residues via dative bonds or covalently via its side-chains. Hemin$^+$ contains a number of relatively long side-chains, and, in the gas phase, some, especially the two propionic acid (PrA) groups, are potentially very flexible. The orientationally averaged collision cross-section (Ω_{avg}, denoted Ω for simplicity hereon) is an indicator of ion structure in the gas phase; typically this property is measured in an ion-mobility (*K*) experiment. The experimental Ω coupled with the theoretical Ω predicted from computationally optimized structures permits insight into the structures of ions in the gas phase, including those ions of biological origin.[5−7]

Here we present our measurements of the Ω of hemin$^+$ and that of a related species, the [Fe^{III}−tetraphenylporphyrin]$^+$ ion (FeTPP$^+$), the structures of which are shown in Figure 1a. The experimental Ω will be compared with the theoretical Ω of structures calculated by means of density functional theory (DFT). The gas-phase structure of hemin$^+$ is expected to be more floppy than that of FeTPP$^+$; many conformers are possible for the two PrA (**PrA1** and **PrA2**) and the aliphatic side-chains. The experimental Ω may thus reflect an average of many rotamers and other low-energy structures. To examine the flexibility of the hemin$^+$ structure, we have also performed some DFT-based molecular dynamics (MD) simulations at a temperature of 300 K. In contrast with hemin$^+$, in FeTPP$^+$, the orientations of the four phenyl groups at the periphery of the porphyrin ring are restricted to minimize steric repulsion between the phenyl and the pyrrolyl hydrogen atoms. FeTPP$^+$ was selected as an ion with few conformers for validating the performance of the theoretical calculations.

Experimental Section

For ion-mobility measurements, 10 μM solutions of hemeproteins (in water or 7:3 water/methanol) and 50 μM solutions of hemin$^+$ (1:1 water/methanol) and FeTPP$^+$ (1:1 acetonitrile/methanol) were prepared. The hemeproteins were horse heart myoglobin and cytochrome *c*; chemicals, including protoporphyrin IX, hemin chloride, meso-tetraphenylporphyrin iron(III) chloride, and HPLC-grade water were all from Sigma-Aldrich (St. Louis, MO). Acetonitrile was from J. T. Baker (Phillipsburg, NJ), and methanol was from Caledon Laboratories (Georgetown, ON, Canada).

Ions were generated from their respective solutions by means of pneumatically assisted electrospray at a typical flow rate of 2 μL/min. The ion-mobility cell is functionally the second quadrupole (q2) of a custom-built triple-quadrupole mass spectrometer, using mostly components from a commercially available API 3000 triple-quadrupole mass spectrometer (MDS SCIEX). The instrumentation has been described in detail elsewhere.[8,9] Briefly, the Q1 and Q3 are conventional MS analyzers; the q2 is a 20-segment quadrupole/ion-mobility cell. Ion injection into the q2 was synchronized with detection, with the arrival times being recorded using a multichannel scaler. Typical ion-mobility measurements were conducted with an axial field of 40−100 V per 20.2 cm in 1 Torr of helium at 298 ± 2 K, giving *E*/*N* values of ∼6−15 Td. Collision cross-sections were calculated using the Mason−Schamp equation:[10,11]

$$\Omega = \left(\frac{3ze}{16N}\right)\left(\frac{2\pi}{\mu kT}\right)^{1/2}\left(\frac{1}{K}\right)$$

where *z* is the numerical charge, *e* is the electronic charge, μ is the reduced mass of the ion and helium, *k* is the Boltzmann constant, and *T* is the temperature. To better determine the presence of unresolved components within an ion-mobility peak, theoretical fitting was performed using a modified version of the software ATCAL, provided by R. R. Hudgins and M. F. Jarrold. ATCAL calculates the diffusion coefficient, *D*, from *K*, via the Einstein equation.[10] When the measured ion-mobility

* Corresponding author. E-mail: kwmsiu@yorku.ca; Fax: (416) 736−5936.

10.1021/jp064873c CCC: $33.50
Published on Web 10/26/2006

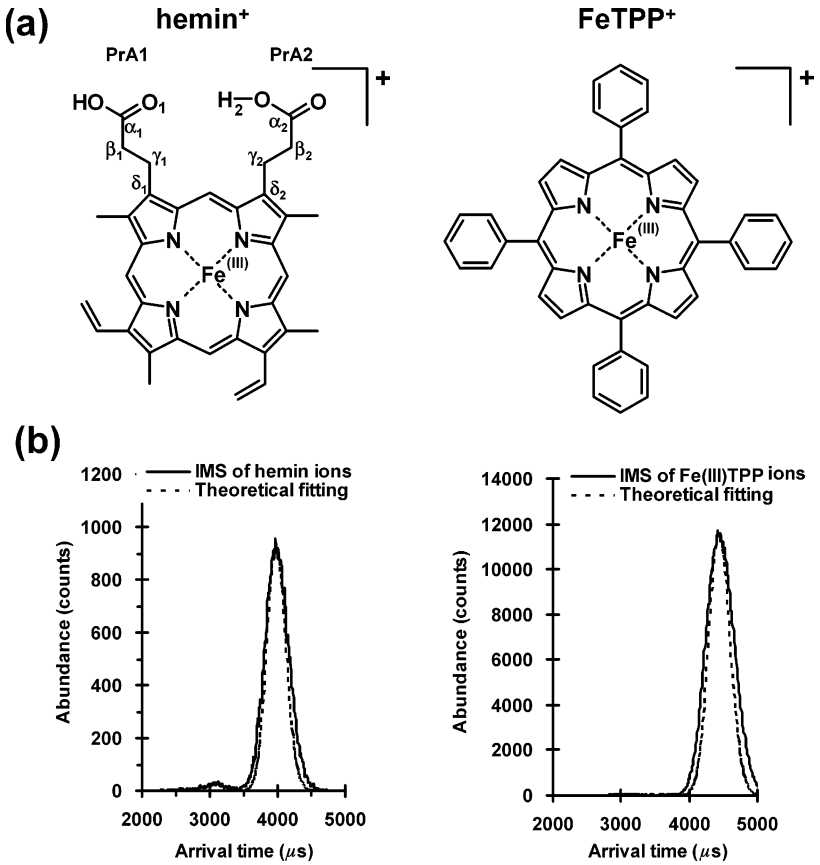

Figure 1. (a) Schematic structures of hemin$^+$ and FeTPP$^+$. (b) Ion-mobility spectra of hemin$^+$ and FeTPP$^+$; the dashed lines show theoretical distributions in which band-broadening is due only to diffusion.

peak is much wider than the theoretical peak, the presence of unresolved structures is indicated.

Computational Details

DFT−MD simulations were carried out using the VASP program (Vienna Ab initio Simulation Package).[12−15] Local density approximation with the Perdew−Wang generalized gradient approximation was used for the exchange-correlation functional.[16] The ground quartet electronic state of hemin$^+$ was calculated by the spin-polarized method. Optimized pseudopotentials for all atoms were constructed by means of the projector augmented wave method.[17] The electronic wave functions were described by a planewave basis set, with the cutoff energy (PW-E_{cutoff}) being 205.42 eV; these were solved by minimizing the total electronic energy at each MD time-step by residual minimization−direct inversion in the iterative subspace. To reduce the interaction between the periodical images imposed by the planewave basis set, an ion was put in a cubic simulation box with a large dimension (22 Å for hemin$^+$ and 25 Å for FeTPP$^+$), and the porphyrin plane was inclined along the diagonal of the cubic box. The DFT−MD simulations on the Born−Oppenheimer potential-energy surface were performed by solving the Newtonian equations of motion with an integration time-step of 0.3 fs. The ion was first heated to 300 K by rescaling the atomic velocities at every MD time-step for a short duration (∼0.2 ps). The MD simulation was then continued with the temperature being kept at 300 K by means of a Nosé−Hoover thermostat.[18] (The simulation time for each DFT−MD run is long enough that the average Ω is converged, with its standard error being smaller than 0.2% as estimated by the block-averaging method.[19])

Geometry optimizations of selected conformers for hemin$^+$ and FeTPP$^+$ were performed by VASP, as described above, as well as by the Gaussian 03 program.[20] For the Gaussian 03 studies, the unrestricted B3LYP hybrid density functional method was used. Two basis sets were employed (BS1: 6-31++G(d,p) for all atoms; BS2: 6-31G(d) for Fe and 6-31G for other atoms). Harmonic frequencies analyses were performed only at the lower UB3LYP/BS2 level. The zero-point, thermal, and entropic corrections at the lower level of theory were used directly for the higher UB3LYP/BS1 level.

Results and Discussion

Figure 1b shows typical ion-mobility spectra of the hemin$^+$ and FeTPP$^+$ ions. The measured Ω are 167 and 188 Å^2, respectively. The hemin$^+$ ions generated from myoglobin and cytochrome *c* (by means of collision-induced dissociation at the interface region) produced ion-mobility peaks and Ω indistinguishable from those generated directly by electrospraying a solution of hemin chloride. Protonated protoporphyrin IX ion, which is hemin$^+$ with the Fe^{3+} ion replaced by three protons, also exhibited the same cross-section (167 Å^2). By comparison, FeTPP$^+$ showed a much larger cross-section. The uncertainty of our experimental values is ±2% or ±3 Å^2. The widths of the peaks were comparable to theoretical widths based on band-broadening due to diffusion, thus indicating the presence of a single isomer or a mixture of isomers having (nearly) identical cross-sections.

The DFT−MD simulation for hemin$^+$ was started from an initial geometry (**Hemin$^+$-1** in Figure 2) that was recently reported by Charkin et al.[1] (at the B3LYP/6-311++G(d,p)//B3LYP/6-31G(d) level of theory) and run for ∼10 ps. This

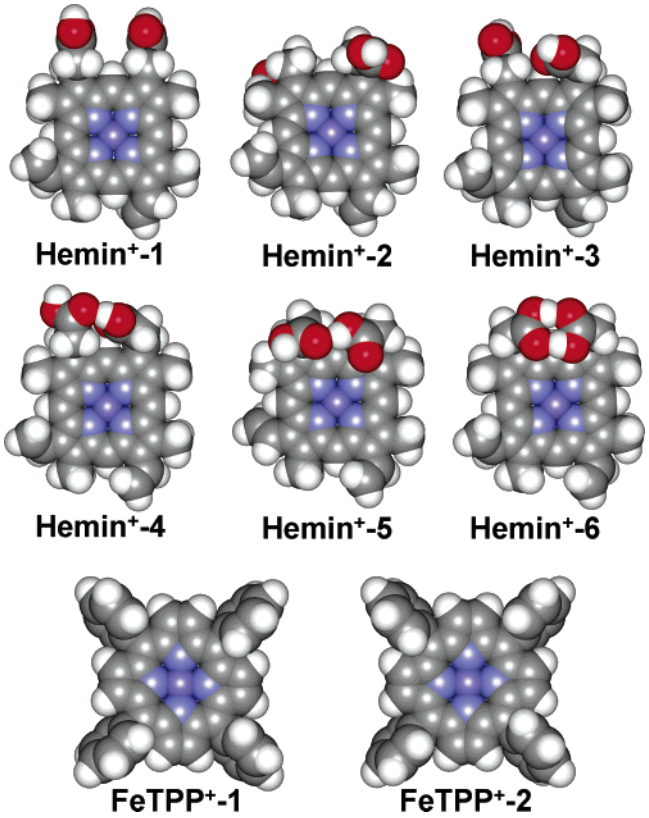

Figure 2. Optimized structures of hemin$^+$ and FeTPP$^+$ employing the UB3LYP/BS2 level (BS2: 6-31G(d) for Fe and 6-31G for other atoms). **Hemin$^+$-1** is the structure obtained by Charkin et al.[1] **Hemin$^+$-2** (2.0 ps), **Hemin$^+$-3** (2.7 ps), and **Hemin$^+$-4** (3.7 ps) are structures selected from the DFT−MD simulation followed by geometry optimization. **Hemin$^+$-5** and **Hemin$^+$-6** are structures similar to **Hemin$^+$-4**: all contain hydrogen bonding between the two PrA side-chains. Energies relative to the respective lowest-energy conformers are listed in Table 1. Atom false colors: dark blue, Fe; blue, N; red, O; gray, C; and white, H.

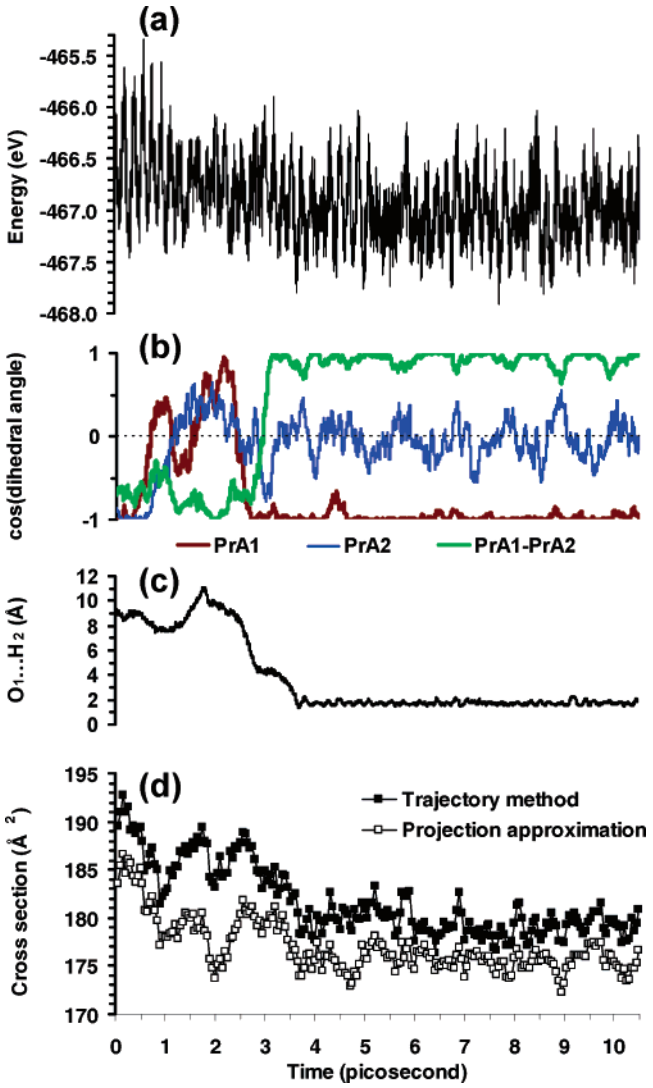

Figure 3. Summary of the DFT−MD simulation (a movie file in mpeg format is provided as Supporting Information). Evolution of (a) energy, (b) the dihedral angle of the PrA side-chain (**PrA1** and **PrA2**) and the relative orientation of the two side-chains (**PrA1-PrA2**), (c) the distance between the carbonyl O on **PrA1** and the hydroxyl H on **PrA2** (hydrogen bond between the two PrA side-chains), and (d) the collision cross-section determined by two models, PA and TM, where each data point is an average cross-section Ω for structures within 50 fs.

initial conformer was found not to have the lowest energy; indeed, a number of more low-lying structures were discovered during the 10-ps DFT−MD run. This is indicated by the energy evolution shown in Figure 3a, where the average energy decreases by approximately 0.6 eV (14 kcal/mol) over the initial 4 ps. The average value then is relatively constant during the remaining simulation, indicating no significant structural change beyond 4 ps. This structural rearrangement largely involves the orientation of the two PrA side-chains. Figure 3b shows the evolution of three dihedral angles: $D_{PrA1} = \alpha_1-\beta_1-\gamma_1-\delta_1$, $D_{PrA2} = \alpha_2-\beta_2-\gamma_2-\delta_2$, and $D_{PrA1-PrA2} = \beta_1-\gamma_1-\gamma_2-\beta_2$. At 0 ps (cf. **Hemin$^+$-1** in Figure 2), both PrA side-chains are trans to the porphyrin ring ($D_{PrA1} = 180°$ and $D_{PrA2} = 180°$), as well as being trans to each other ($D_{PrA1-PrA2} = 180°$). Bonds are then rotated until an equilibrium structure ($D_{PrA1} = 180°$, $D_{PrA2} = 90°$, and $D_{PrA1-PrA2} = 0°$) is reached after ∼3 ps (cf. **Hemin$^+$-4** in Figure 2). At the same time, a hydrogen bond between the two carboxylic groups is formed (Figure 3c). A movie of the DFT-MD trajectory is provided as Supporting Information.

On the basis of the DFT−MD trajectory of hemin$^+$, the geometries of some representative conformers were selected and optimized by VASP and Gaussian 03 programs (Figure 2). **Hemin$^+$-1** (0.0 ps) is the Charkin structure, with the two PrA side-chains pointing away from the porphyrin ring.[1] By contrast, both PrA side-chains in **Hemin$^+$-2** (2.0 ps) bend back to the porphyrin ring, but on opposite faces. The **PrA1** of **Hemin$^+$-3** (2.7 ps) is similar to that in **Hemin$^+$-1**, while the **PrA2** is perpendicular to the former. **Hemin$^+$-4** (beyond 3.7 ps) exhibits an intramolecular hydrogen bond between the two carboxylic groups. The formation of such intramolecular hydrogen bonding has also been proposed very recently by Charkin et al.[21] in a deprotonated hemin neutral complex. For comparison, two additional structures were optimized, **Hemin$^+$-5** and **Hemin$^+$-6**, which contain one and two hydrogen bonds, respectively. Two conformers of FeTPP$^+$ (**FeTPP$^+$-1** and **FeTPP$^+$-2**, differing by the orientation of the phenyl rings) were also optimized and are shown in Figure 2.

The energies of the hemin$^+$ and FeTPP$^+$ isomers, relative to their respective lowest-energy conformers, are shown in Table 1. The VASP energies (ΔE) show that improving the accuracy of the planewave basis set by increasing the PW-E_{cutoff} from 205.42 to 273.89 eV has little effect on the relative energies. The relative energies are also in excellent agreement with those evaluated at the UB3LYP/6-31++G(d,p) level. As expected, differences between the corrections for the zero-point and thermal energies (ΔE_{ZPC} and ΔH, respectively) within a given

TABLE 1. Relative Energies (kcal mol^{-1}) and Collision Cross-Section Ω (Å^2) of hemin$^+$ and FeTPP$^+$[†]

VASP GGA	PW-E_{cutoff} = 273.89 eV				PW-E_{cutoff} = 205.42 eV			
	Rel. energy / kcal mol^{-1}	Cross section[b] / Å^2 (% diff.)[d]			Rel. energy / kcal mol^{-1}	Cross section[b] / Å^2 (% diff.)[d]		
	ΔE	PA	EHSS	TM	ΔE	PA	EHSS	TM
Hemin$^+$-1[a]	13.0	181 (8.4)	199 (18.9)	185 (10.9)	13.3	183 (9.7)	201 (20.1)	187 (11.7)
Hemin$^+$-2	10.6	178 (6.4)	197 (17.7)	185 (10.8)	10.5	179 (7.0)	198 (18.4)	186 (11.6)
Hemin$^+$-3	11.7	179 (7.2)	198 (18.4)	185 (10.8)	10.6	181 (8.3)	200 (19.8)	188 (12.3)
Hemin$^+$-4	4.8	173 (3.4)	188 (12.6)	176 (5.4)	3.8	174 (4.5)	190 (13.9)	177 (6.0)
Hemin$^+$-5	9.3	169 (1.2)	186 (11.2)	175 (4.6)	8.3	170 (2.0)	187 (11.8)	177 (5.8)
Hemin$^+$-6	0.0	168 (0.7)	183 (9.8)	173 (3.4)	0.0	170 (1.8)	185 (10.9)	174 (4.3)
FeTPP$^+$-1	0.0	190 (1.0)	210 (11.7)	196 (4.4)	0.0	192 (2.2)	212 (12.9)	198 (5.4)
FeTPP$^+$-2	0.1	190 (1.0)	211 (12.0)	196 (4.3)	0.1	192 (2.1)	213 (13.2)	199 (5.8)
Gaussian03 B3LYP	BS1: 6-31++G(d,p)				BS2: H,C,N,O:6-31G; Fe:6-31G(d)			
	Rel. energy / kcal mol^{-1}				Rel. energy / kcal mol^{-1}			
	ΔE	ΔE_{ZPC}[c]	ΔH[c]	ΔG[c]	ΔE	ΔE_{ZPC}[c]	ΔH[c]	ΔG[c]
Hemin$^+$-1[a]	8.5	7.1	8.2	3.2	14.9	13.5	14.6	9.5
Hemin$^+$-2	4.6	3.7	4.4	1.8	9.3	8.3	9.0	6.4
Hemin$^+$-3	8.5	7.4	8.2	5.4	11.8	10.7	11.5	8.7
Hemin$^+$-4	0.9	0.7	1.0	0.8	2.1	2.0	2.3	2.1
Hemin$^+$-5	4.3	4.1	4.4	3.6	6.5	6.2	6.6	5.8
Hemin$^+$-6	0.0	0.0	0.0	0.0	0.0	0.0	0.0	0.0
FeTPP$^+$-1					0.0	0.0	0.0	0.0
FeTPP$^+$-2					0.1	0.1	0.1	-0.1

	Cross section[b] / Å^2 (% diff.)[d]			
Experiment		VASP-MD PW-E_{cutoff} = 205.42 eV		
		PA[e]	EHSS[e]	TM[e]
hemin$^+$	167 ± 3	Hemin$^+$-4 175.6 ± 1.1 (5.1)	191.6 ± 1.5 (14.8)	179.4 ± 1.4 (7.4)
		Hemin$^+$-6 171.2 ± 1.1 (2.5)	186.9 ± 1.5 (11.9)	175.9 ± 1.4 (5.3)
FeTPP$^+$	188 ± 3	FeTPP$^+$ 192.0 ± 0.8 (2.1)	212.9 ± 1.2 (13.2)	198.8 ± 1.3 (5.8)

[†] Numbers in parentheses are the percentage differences of the theoretical Ω from the experimental values [a] Structure of Charkin et al. [b] Cross-sections are calculated by PA, EHSS, and TM. [c] Zero-point, thermal, and entropic corrections at the UB3LYP/BS2 level are used. [d] % difference from experimental Ω. [e] The uncertainty is one standard deviation from the average Ω obtained by the DFT−MD simulations.

conformer are almost identical across the six conformers because the structures differ only by rotation about bonds. The relative energies are consistent with the results of DFT−MD simulation, in which hydrogen bonding is eventually formed.

To correlate theory with experiments, the theoretical Ω of the above hemin$^+$ structures were calculated using three models: projection approximation (PA),[22] exact hard sphere scattering (EHSS),[23] and trajectory method (TM).[24] These models were all available from the MOBCAL program suite, courtesy of M. F. Jarrold.[25] The results of these calculations are summarized in Table 1. The Ω obtained by different models show large differences, with EHSS typically being much larger than the PA and TM values. We have found in the past that, for biological ions, Ω calculated using PA and TM are closer to experimental Ω than those calculated using EHSS.[8,26] The theoretical Ω of **FeTPP$^+$-1** and **FeTPP$^+$-2** are identical, consistent with the rigid structure of FeTPP$^+$. The PA value of 190 Å^2 and the TM value of 196 Å^2, based on the UB3LYP/BS2 structures, are respectively 1 and 4% larger than the experimental Ω of 188 Å^2. By contrast, the Ω values of the various hemin$^+$ conformers are different and depend on the orientations of the two PrA side-chains. Those isomers without intramolecular hydrogen bonding (**Hemin$^+$-1**, **Hemin$^+$-2** and **Hemin$^+$-3**) are approximately 10 Å^2 larger than those with it (**Hemin$^+$-4**, **Hemin$^+$-5** and **Hemin$^+$-6**). For **Hemin$^+$-6**, the lowest-energy conformer, the PA value of 168 Å^2 and the TM value of 173 Å^2 (UB3LYP/6-31++G(d,p)) differ from the experimental Ω of 167 Å^2 by 1 and 4%, respectively. For **Hemin$^+$-4**, which is calculated to lie above **Hemin$^+$-6** by only 0.8 kcal/mol in relative free energy, the PA Ω of 172 Å^2 and the TM Ω of 176 Å^2 are larger than the experimental Ω by 3 and 5%, respectively. As the imprecision of ion-mobility measurements is typically ±2% (approximately ±3 Å^2) and the thermal effect on Ω revealed by DFT−MD simulations is 2 Å^2 (see below), the ion-mobility peaks corresponding to the conformers **Hemin$^+$-4** and **Hemin$^+$-6** are experimentally unresolvable. Assuming Boltzmann distribution (**Hemin$^+$-4**/**Hemin$^+$-6** ≈ 1/4), the population-averaged Ω is 169 Å^2 (PA) and 174 Å^2 (TM). Thus, there is good general agreement between experiment (167 Å^2) and theory.

The evolution of Ω, calculated by the PA and TM methods, in the DFT−MD simulation is shown in Figure 3d. The trend of Ω decreasing during structural rearrangement is evident. From the last 7 ps of the DFT−MD run, one can calculate an average Ω for **Hemin$^+$-4** to be 176 ± 1 Å^2 (PA) and 179 ± 1 Å^2 (TM), where the uncertainties are one standard deviation from the average Ω. Thermal molecular vibration at 300 K raises the average Ω of hemin$^+$ by a few Å^2 above the Ω of the static structure optimized at the same computational condition (PW-E_{cutoff} = 205.42 eV). The same thermal effect is also observed in a DFT−MD simulation with the lowest-energy conformer, **Hemin$^+$-6**, as an initial structure for which an average Ω is calculated to be 171 ± 1 Å^2 (PA) and 176 ± 1 Å^2 (TM). By contrast, DFT−MD simulation for the more rigid FeTPP$^+$ gives an average Ω identical to the Ω of the optimized structure. This indicates that thermal effect is important to the Ω of an ion with a flexible structure. It may also be of interest to note the differences in Ω obtained by the different levels of theory used in this study. The Ω values obtained from the VASP structures calculated with PW-E_{cutoff} = 205.42 eV (the condition for the DFT−MD simulation) are approximately 2 Å^2 larger than those calculated with PW-E_{cutoff} = 273.89 eV; the latter are closer to those values obtained from the UB3LYP structures. All results

strongly suggest that, at 300 K, hemin$^+$ has internal hydrogen bonding between the two propionic groups.

A reviewer of this article questioned the interconversion between conformers and, in particular, that between **Hemin$^+$-4** and **Hemin$^+$-6**. Our experience in the electrospray mass spectrometry of biomolecules is that interconversion of rotamers with intramolecular hydrogen bonding is efficient and that there is efficient thermalization of ions in the lens and q0 regions.[27−34] The collisional heating largely experienced near the front of the lens/q0 region and downstream collisional cooling results in "annealing" of the sampled ions.[31−33] The assumption of Boltzmann distribution above was employed out of expediency and, in reality, poor understanding of the collisional and transport properties of the ions in these regions. In addition, another uncertainty arises from the accuracy of DFT calculations employed, which has generally been accepted to be ±2−3 kcal/mol (although the relative energies among isomers are probably much better than this limit).[29,35,36] Thus, there is considerable room for error in the value of population-averaged Ω, although, in reality, this is minimized by the small difference of 3−4 Å^2 between **Hemin$^+$-4** and **Hemin$^+$-6**. Conversion between the two conformers has not been observed in our DFT−MD runs less than 20 ps in duration. DFT−MD runs significantly longer than 20 ps are currently intractable using our high-performance computing resources. In reality, all MD runs are necessarily short relative to the transit (annealing) time of hemin$^+$ ions through the lens/q0 region (on the order of milliseconds).

Acknowledgment. The DFT−MD calculations were performed on a computer cluster on SHARCNET. We thank Martin F. Jarrold and Robert R. Hudgins for making available to us the mobility software programs, MOBCAL and ATCAL. Funding from NSERC, MDS SCIEX and York University is gratefully acknowledged.

Supporting Information Available: Movie of the DFT-MD trajectory. This material is available free of charge via the Internet at http://pubs.acs.org.

References and Notes

(1) Charkin, O. P.; Klimenko, N. M.; Nguyen, P. T.; Charkin, D. O.; Mebel, A. M.; Lin, S. H.; Wang, Y. S.; Wei, S. C.; Chang, H. C. *Chem. Phys. Lett.* **2005**, *415*, 362−369.

(2) Nonose, S.; Tanaka, H.; Okai, N.; Shibakusa, T.; Fuke, K. *Eur. Phys. J. D* **2002**, *20*, 619−626.

(3) Nonose, S.; Iwaoka, S.; Mori, K.; Shibata, Y.; Fuke, K. *Eur. Phys. J. D* **2005**, *34*, 315−319.

(4) Angelelli, F.; Chiavarino, B.; Crestoni, M. E.; Fornarini, S. *J. Am. Soc. Mass Spectrom.* **2005**, *16*, 589−598.

(5) Clemmer, D. E.; Hudgins, R. R.; Jarrold, M. F. *J. Am. Chem. Soc.* **1995**, *117*, 10141−10142.

(6) Hoaglund-Hyzer, C. S.; Counterman, A. E.; Clemmer, D. E. *Chem. Rev.* **1999**, *99*, 3037−3079.

(7) Wyttenbach, T.; von Helden, G.; Bowers, M. T. *J. Am. Chem. Soc.* **1996**, *118*, 8355−8364.

(8) Guo, Y. Z.; Ling, Y.; Thomson, B. A.; Siu, K. W. M. *J. Am. Soc. Mass Spectrom.* **2005**, *16*, 1787−1794.

(9) Guo, Y. Z.; Wang, J. X.; Javahery, G.; Thomson, B. A.; Siu, K. W. M. *Anal. Chem.* **2005**, *77*, 266−275.

(10) Mason, E. A.; McDaniel, E. W. In *Transport Properties of Ions in Gases*; John Wiley & Sons: New York, 1988.

(11) Revercomb, H. E.; Mason, E. A. *Anal. Chem.* **1975**, *47*, 970−983.

(12) Kresse, G.; Hafner, J. *Phys. Rev. B* **1993**, *47*, 558−561.

(13) Kresse, G.; Hafner, J. *Phys. Rev. B* **1994**, *49*, 14251−14269.

(14) Kresse, G.; Furthmuller, J. *Comput. Mater. Sci.* **1996**, *6*, 15−50.

(15) Kresse, G.; Furthmuller, J. *Phys. Rev. B* **1996**, *54*, 11169−11186.

(16) Perdew, J. P.; Wang, Y. *Phys. Rev. B* **1992**, *45*, 13244−13249.

(17) Blöchl, P. E. *Phys. Rev. B* **1994**, *50*, 17953−17979.

(18) Nosé, S. *J. Chem. Phys.* **1984**, *81*, 511−519.

(19) Flyvbjerg, H.; Petersen, H. G. *J. Chem. Phys.* **1989**, *91*, 461−466.

(20) Frisch, M. J.; Trucks, G. W.; Schlegel, H. B.; Scuseria, G. E.; Robb, M. A.; Cheeseman, J. R.; Montgomery, J. A., Jr.; Vreven, T.; Kudin, K. N.; Burant, J. C.; Millam, J. M.; Iyengar, S. S.; Tomasi, J.; Barone, V.; Mennucci, B.; Cossi, M.; Scalmani, G.; Rega, N.; Petersson, G. A.; Nakatsuji, H.; Hada, M.; Ehara, M.; Toyota, K.; Fukuda, R.; Hasegawa, J.; Ishida, M.; Nakajima, T.; Honda, Y.; Kitao, O.; Nakai, H.; Klene, M.; Li, X.; Knox, J. E.; Hratchian, H. P.; Cross, J. B.; Bakken, V.; Adamo, C.; Jaramillo, J.; Gomperts, R.; Stratmann, R. E.; Yazyev, O.; Austin, A. J.; Cammi, R.; Pomelli, C.; Ochterski, J. W.; Ayala, P. Y.; Morokuma, K.; Voth, G. A.; Salvador, P.; Dannenberg, J. J.; Zakrzewski, V. G.; Dapprich, S.; Daniels, A. D.; Strain, M. C.; Farkas, O.; Malick, D. K.; Rabuck, A. D.; Raghavachari, K.; Foresman, J. B.; Ortiz, J. V.; Cui, Q.; Baboul, A. G.; Clifford, S.; Cioslowski, J.; Stefanov, B. B.; Liu, G.; Liashenko, A.; Piskorz, P.; Komaromi, I.; Martin, R. L.; Fox, D. J.; Keith, T.; Al-Laham, M. A.; Peng, C. Y.; Nanayakkara, A.; Challacombe, M.; Gill, P. M. W.; Johnson, B.; Chen, W.; Wong, M. W.; Gonzalez, C.; Pople, J. A. *Gaussian 03*, revision D.01; Gaussian, Inc.: Wallingford, CT, 2004.

(21) Charkin, O. P.; Klimenko, N. M.; Charkin, D. O.; Wang, Y. S.; Wei, S. C.; Chang, H. C.; Lin, S. H. *Russ. J. Inorg. Chem.* **2006**, *51*, 89−98.

(22) von Helden, G.; Hsu, M. T.; Gotts, N.; Bowers, M. T. *J. Phys. Chem.* **1993**, *97*, 8182−8192.

(23) Shvartsburg, A. A.; Jarrold, M. F. *Chem. Phys. Lett.* **1996**, *261*, 86−91.

(24) Mesleh, M. F.; Hunter, J. M.; Shvartsburg, A. A.; Schatz, G. C.; Jarrold, M. F. *J. Phys. Chem.* **1996**, *100*, 16082−16086.

(25) Jarrold, M. F. Mobcal Website. http://nano.chem.indiana.edu/Software.html (accessed Jan 2004).

(26) Rodriquez, C. F.; Orlova, G.; Guo, Y. Z.; Li, X. M.; Siu, C. K.; Hopkinson, A. C.; Siu, K. W. M. *J. Phys. Chem. B* **2006**, *110*, 7528−7537.

(27) Rodriquez, C. F.; Cunje, A.; Shoeib, T.; Chu, I. K.; Hopkinson, A. C.; Siu, K. W. M. *J. Am. Chem. Soc.* **2001**, *123*, 3006−3012.

(28) El Aribi, H.; Shoeib, T.; Ling, Y.; Rodriquez, C. F.; Hopkinson, A. C.; Siu, K. W. M. *J. Phys. Chem. A* **2002**, *106*, 2908−2914.

(29) El Aribi, H.; Rodriquez, C. F.; Shoeib, T.; Ling, Y.; Hopkinson, A. C.; Siu, K. W. M. *J. Phys. Chem. A* **2002**, *106*, 8798−8805.

(30) El Aribi, H.; Rodriquez, C. F.; Almeida, D. R. P.; Ling, Y.; Mak, W. W.-N.; Hopkinson, A. C.; Siu, K. W. M. *J. Am. Chem. Soc.* **2003**, *125*, 9229−9236.

(31) Douglas, D. J. *J. Phys. Chem.* **1982**, *86*, 185−191.

(32) Dawson, P. H.; French, J. B.; Buckley, J. A.; Douglas, D. J.; Simmons, D. *Org. Mass Spectrom.* **1982**, *17*, 205−211.

(33) Douglas, D. J.; French, J. B. *J. Am. Soc. Mass Spectrom.* **1992**, *3*, 398−408.

(34) Anderson, S. G.; Blades, A. T.; Klassen, J.; Kebarle, P. *Int. J. Mass Spectrom. Ion Processes* **1995**, *141*, 217−228.

(35) Boys, S. F.; Bernardi, F. *Mol. Phys.* **1970**, *19*, 553−566.

(36) Ketvirtis, A. E.; Bohme, D. K.; Hopkinson, A. C. *J. Phys. Chem.* **1995**, *99*, 16121−16127.